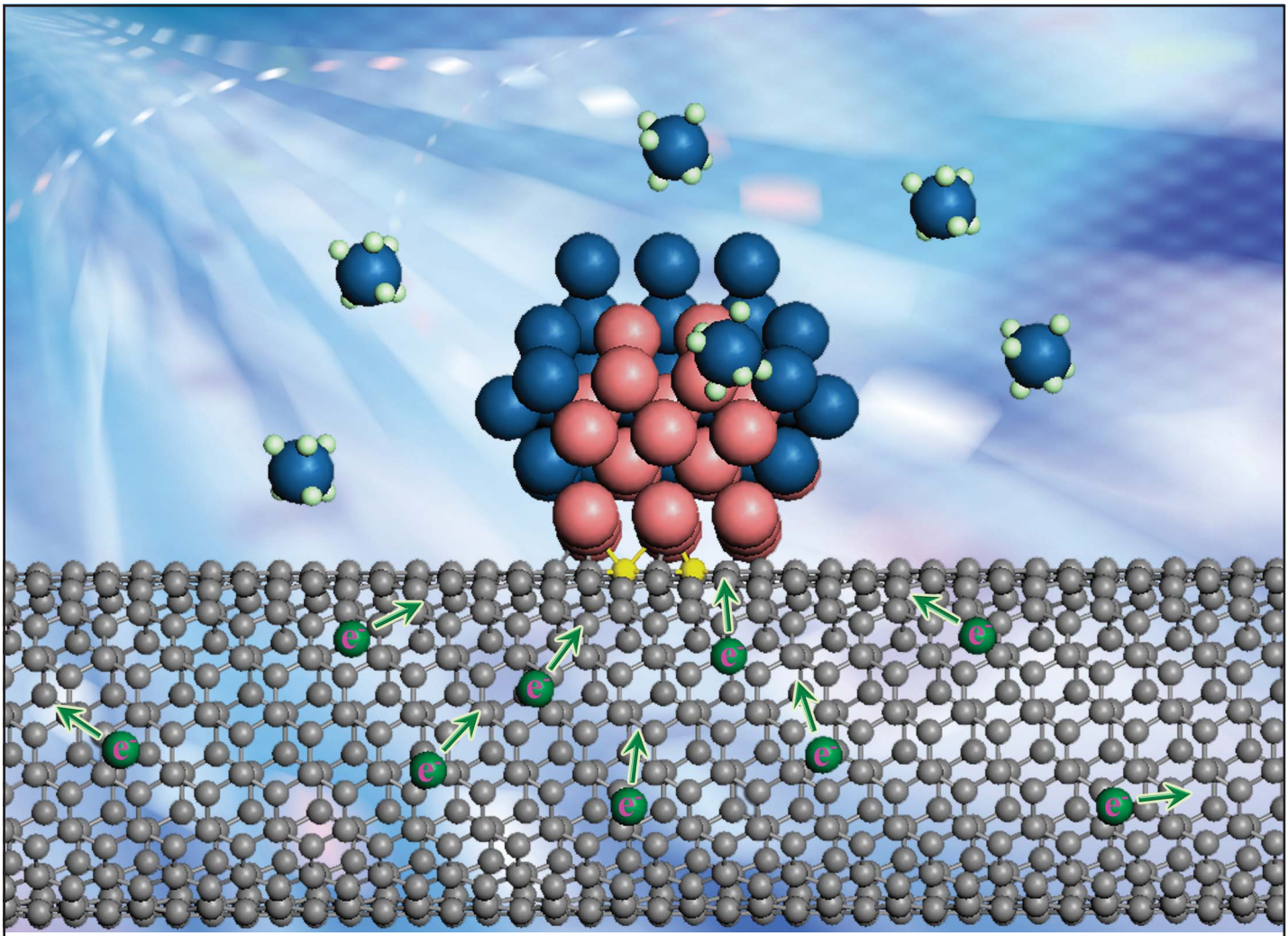

A common interest pushes forward the development of a novel fuel cell electrode material, leveraging a partnership between the two nanomaterial groups of Prof. Zidong Wei at Chongqing University and Prof. Li-Jun Wan at the Institute of Chemistry, the Chinese Academy of Sciences.

Title: Pd-induced Pt(IV) reduction to form Pd@Pt/CNT core@shell catalyst for a more complete oxygen reduction

This work introduces a facile and controllable process for preparing Pd@Pt/CNT core@shell catalysts for the oxygen reduction reaction (ORR) *via* Pd-induced Pt(IV) reduction on Pd/CNT. The mass-specific activity for the ORR of the Pd@Pt/CNT catalysts is 7–9 times higher than that of the state-of-the-art Pt/C catalysts, but the yield of the harmful species H_2O_2 of the former is only 14.1% of that of the latter.

As featured in:

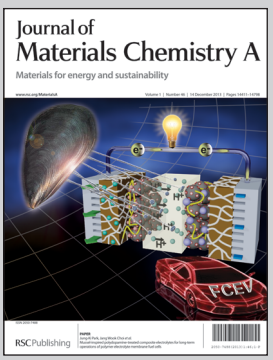

See M. Xia *et al.*,
J. Mater. Chem. A, 2013, **1**, 14443.

RSC Publishing

www.rsc.org/MaterialsA

Registered Charity Number 207890

Journal of Materials Chemistry A

RSC Publishing

COMMUNICATION

View Article Online
View Journal | View Issue

Cite this: *J. Mater. Chem. A*, 2013, **1**, 14443

Received 9th August 2013
Accepted 27th September 2013

DOI: 10.1039/c3ta13139d

www.rsc.org/MaterialsA

Pd-induced Pt(IV) reduction to form Pd@Pt/CNT core@shell catalyst for a more complete oxygen reduction†

Meirong Xia,[a] Ying Liu,[a] Zidong Wei,*[a] Siguo Chen,[a] Kun Xiong,[a] Li Li,[a] Wei Ding,[a] Jinsong Hu,[b] Li-Jun Wan,*[b] Rong Li[a] and Shahnaz Fatima Alvia[a]

We describe a facile and controllable process for preparing Pd@Pt/CNT core@shell catalysts for the oxygen reduction reaction (ORR) *via* Pd-induced Pt(IV) reduction on Pd/CNT. The mass-specific activity for the ORR of the Pd@Pt/CNT catalysts is 7–9 times higher than that of the state-of-the-art Pt/C catalysts, but the yield of H_2O_2, a harmful species for the stability of catalysts, of the former is only 14.1% of that of the latter. The reason for the enhanced activity and the lower H_2O_2 yield on the Pd@Pt/CNT catalysts was studied by DFT calculations.

Introduction

Proton exchange membrane fuel cells (PEMFCs) are considered to be a promising method for powering electric vehicles. The Pt/C catalyst remains the state-of-the-art, at least for acid-based fuel cells, despite many attempts to create a non-Pt catalyst for low-temperature (<200 °C) air cathodes. However, two drawbacks of the Pt/C catalyst prevent its commercial application: the high cost of Pt at the amount currently required,[1] and its activity deterioration with use. The deterioration mechanisms of the Pt/C cathode catalyst can be summarized as follows:[2–5] (1) Pt nanoparticles dissolve and subsequently undergo Oswald ripening; (2) the Pt nanoparticles aggregate driven by surface-energy minimization; (3) Pt nanoparticles are lost due to corrosion of the carbon support. Ultimately, the deterioration of the Pt/C cathode catalyst can largely be attributed to H_2O_2 species, an intermediate of the oxygen reduction reaction (ORR) at the cathode. It is currently accepted that H_2O_2 causes Pt nanoparticles to oxidize and dissolve, with subsequent Oswald ripening and loss of the carbon support due to corrosion. Therefore, a catalyst with low Pt usage and reduced H_2O_2 production must be developed before the commercialization of PEMFCs becomes possible. Many studies have attempted to reduce the H_2O_2 production of the ORR.[6–9] The use of transition metals, such as Fe, Co, Ni and Cu,[10–12] and noble metals, including Au, Ag, Ru and Pd, has been reported in Pt-based bimetallic catalysts, among which Pt–Pd catalysts exhibit the best activity for the ORR.[13–16] Pd–Pt bimetallic nano-dendrites reportedly exhibit 2.5 times higher activity for the ORR than the state-of-the-art Pt/C catalyst.[17–20] A promising approach involves creating an alloy of Pt with Pd using a sequential synthesis method and/or co-reduction, *etc.*[21–25] Another approach involves varying the shape and morphology of the Pt–Pd bimetallic nanocomposites.[26–28] Core@shell or core@shell-like bimetallic catalysts provide a wide range of possibilities by substituting either the core metal or a portion of the Pt monolayer shell with Pd.[19,29] Adzic *et al.* reported a series of studies on the ORR activity of Pd–Pt monolayer core@shell catalysts which were synthesized *via* Cu underpotential deposition followed by galvanic displacement of the Cu adatoms.[19,20,30] The Pt mass-specific ORR activity of the Pd(core)–Pt(shell)/C was reportedly 5–8 times higher than that of the Pt/C catalyst.[31] However, the current procedure for fabricating core@shell catalysts is complicated and time consuming. In particular, the under-potential deposition (UPD) technique is not easy to handle. In fact, the UPD technique only works on an electrode, not on discrete catalyst support particles.[32,33] Thus, the UPD technique cannot be applied for mass production.

In this work, we used a unique approach of Pt self-reduction catalyzed by Pd previously deposited on carbon nanotubes (CNTs) to synthesize a Pd@Pt/CNT core@shell catalyst. The present synthetic method provides a convenient and environmentally benign route to the large-scale production of Pd@Pt/CNT core@shell catalysts because it does not require an electrochemical UPD technique. Density functional theory (DFT) calculations validate the finding that the Pd@Pt/CNT shows improved catalysis of the ORR and produces less H_2O_2 than the conventional Pt/C catalysts given the adsorption energy of all

[a]*The State Key Laboratory of Power Transmission Equipment & System Security and New Technology, College of Chemistry and Chemical Engineering, Chongqing University, Chongqing, 400044, China. E-mail: zdwei@cqu.edu.cn; Fax: +86-23-65102531*

[b]*Institute of Chemistry, The Chinese Academy of Sciences, Beijing, 100190, China. E-mail: wanlijun@iccas.ac.cn; Fax: +86-010-62751700*

† Electronic supplementary information (ESI) available. See DOI: 10.1039/c3ta13139d

oxygen-containing species and the barrier energy of HO–O bond dissociation. The ORR activity of the Pd@Pt/CNT catalysts was enhanced by weakening the adsorption of the oxygen-containing species and by weakening the HO–O bond strength more than that of the pure metallic catalysts Pt/CNT and Pd/CNT.

Results and discussion

To improve the Pd dispersity and stability on the CNTs, the CNTs were functionalized with thiol groups according to our previous report.[34,35] CNTs have abundant free-flowing π electrons, which make them potential reductants for reactions that require electrons. As long as an energy difference is maintained for the electrons between the CNT and the Pt^{4+} ions, electrons are spontaneously transferred from the CNT to the Pt^{4+} ions, which leads to a reduction of the Pt^{4+} ions. In general, Pt^{4+} ions may be reduced at any site on a CNT. However, the Pt^{4+} ions may be preferentially reduced around Pd particles due to the catalytic action of the Pd. Therefore, the Pd@Pt/CNT catalysts were formed according to the schematic diagram in Fig. 1. The synthesis of Pd/CNT was readily achieved using sodium borohydride and trisodium citrate as a reducing reagent and a protective stabilizer, respectively. The Pd particles, previously reduced on thiolated CNT, were used as seeds and catalysts for Pt deposition and growth, and therefore prevented the Pt deposits from being randomly distributed along the entire CNT. The as-prepared Pd/CNT was immersed into a H_2PtCl_6 solution without any reducing reagent. The Pt^{4+} ions were reduced by the electrons from the CNT with Pd catalysis. Thus, the Pt NPs were preferentially deposited around the Pd NPs. The Pt shell was modulated by the content of the H_2PtCl_6 solution. The Fermi level for an electron in the $PtCl_6^{2-}$/Pt redox couple is 0.74 eV, but it is +0.5 eV in the CNT.[30] Therefore, an electron can transfer from the CNT to the $PtCl_6^{2-}$/Pt redox pair. The Pd@Pt/CNT structures were finally obtained, and the Pd@Pt/CNT catalyst prepared with a Pd : Pt atomic ratio of $n:m$ is labelled $Pd_n@Pt_m$/CNT. The real ratios of Pd : Pt in the final products was determined *via* inductively coupled plasma atomic emission spectroscopy (ICP-AES), which are in good agreement with the designated values, as shown in Table S1.† This means the reduction of Pt^{4+} and Pd^{2+} ions is complete in the designed method.

The synthesized $Pd_4@Pt_1$/CNT, $Pd_2@Pt_1$/CNT, and Pd/CNT catalysts were characterized *via* XRD as shown in Fig. S1.† The crystallographic analysis of the Pd/CNT revealed three peaks, corresponding to the (111), (200), and (220) reflections of face-centered cubic palladium (*Fm3m*, JCPDS no. 46-1043). The XRD peaks of $Pd_4@Pt_1$/CNT and $Pd_2@Pt_1$/CNT appear between those of the pure Pd and Pt metals. In the Pd_n–Pt_m/CNT, as the Pt content increases the XRD peaks begin to deviate from those of the pure Pd to those of the pure Pt [*Fm3m*, JCPDS no. 04-0802]. Belonging to the same elemental group, Pt and Pd share similar XRD characteristics. The particle sizes of the catalysts estimated by the Scherrer equation were 4.6 and 3.6 nm for $Pd_2@Pt_1$/CNT and Pd/CNT, respectively, which are in agreement with the average particle sizes estimated *via* TEM.

Fig. S2† shows the typical TEM images of the (a) Pd/CNT and (b) $Pd_2@Pt_1$/CNT. The as-prepared Pd/CNT (Fig. S2a†) and $Pd_2@Pt_1$/CNT (Fig. S2b†) are relatively uniform with average diameters of 3.6 and 4.6 nm, respectively. The HRTEM image of the $Pd_2@Pt_1$/CNT is shown in Fig. S2c† and clearly indicates a core@shell structure with interplanar spacings of 0.194 and 0.225 nm for the Pd core. The measured interplanar spacing of the Pt shell lattice was 0.223 nm, which corresponds to the (111) lattice plane of face-centered cubic (fcc) Pt. The fast Fourier transform (FFT) pattern (Fig. S2d†) of the HRTEM image (Fig. S2c,† the ring portions) indicates that the electron diffraction ring was ascribed to Pt with the lattice planes (200), (111), (220), (311) and (331).

The elemental distributions of $Pd_2@Pt_1$/CNT were analyzed *via* high-angle annular dark field scanning TEM (HAADF-STEM) (Fig. 2a and b). The elemental map clearly indicates that the Pd (presented in red) is either neighboring (site (1)) or covered by (site (2)) the Pt (presented in orange). A portion of the Pt can also be reduced at site (3), at which position no Pd was previously deposited. Obviously, the reduction of the Pt ions occurs preferentially around the Pd particles. The dendritic growth of the Pt shell can likely be attributed to the higher rate of Pt growth on the Pt surface than on the Pd due to the lower activation energy for the growth of Pt on Pt than that on other metal

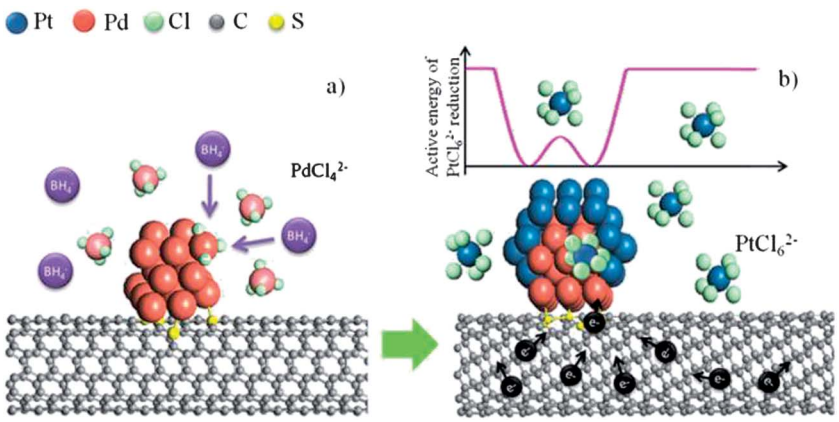

Fig. 1 (a) The formation of Pd/CNT, and (b) the synthesis of Pd@Pt/CNTs.

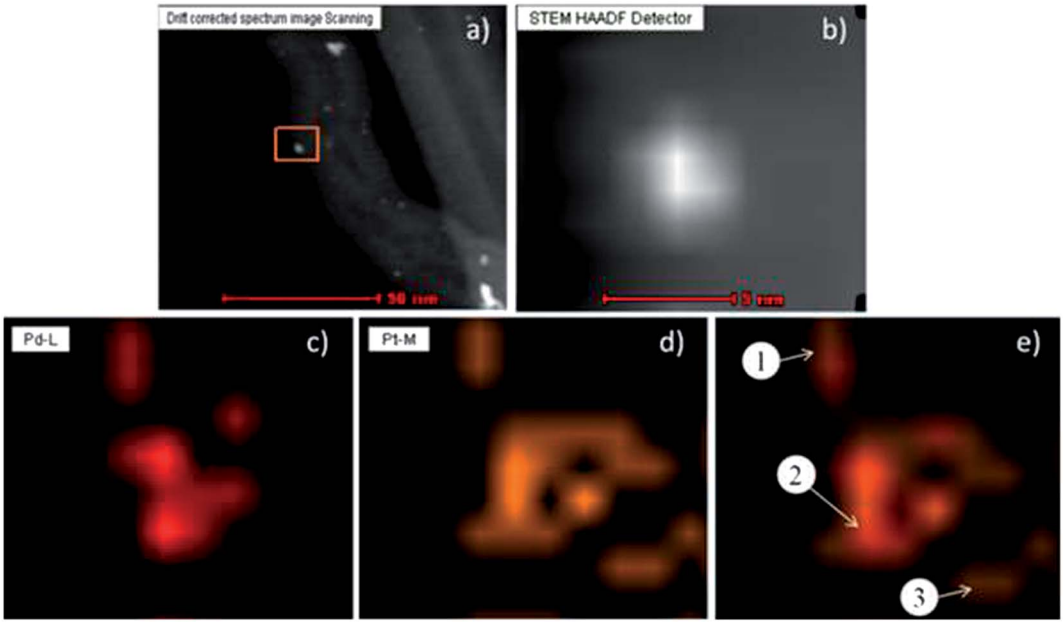

Fig. 2 HAADF-STEM mapping images of the $Pd_2@Pt_1$/CNTs (a and b). The cross-sectional compositional line profiles of (c) Pd–L, (d) Pt–M, and (e) the overlap of the Pd–L (c) and Pt–M (d).

substrates.[36–40] These results are in agreement with the previous observation of Pt deposition on Pd crystals.[18] The surface was found to be composed of Pt islands with exposed bare Pd surfaces. Fortunately, a Pt crystal with a dendritic structure is more conducive to the catalysis of the ORR than that with a spherical structure.[18]

After the Pd/CNT and CNT samples were immersed in a H_2PtCl_6 solution, separately, 2 mL of the suspension was removed every hour to determine the Pt(IV) content *via* UV spectrophotometry. The results are presented in Fig. S3.† The Pt^{4+} ion content remaining in the H_2PtCl_6 solution containing Pd/CNT decreased more rapidly than that with the CNT, indicating that although a reduction of the Pt^{4+} ions can spontaneously occur on the CNT, it can be accelerated by the presence of Pd.

The performance of the Pd@Pt/CNT is presented in Fig. 3 together with those of Pt/C (John-Matthew Co., UK) and Pd/CNT for comparison, and the half-wave potentials of the ORR and the H_2O_2 yield are listed in Table 1.

Fig. 3 and Table 1 demonstrate that the three electrodes made from Pd@Pt/CNT bimetallic nanocatalysts display a more positive ORR onset and half-wave potential with smaller H_2O_2 yields than the state-of-the-art Pt/C catalysts, indicating improved catalytic performance for a four-electron reduction of the ORR. To evaluate the intrinsic activity of the Pd@Pt/CNT samples, the kinetic current at 0.9 V was normalized to the loading quantity of the metals (Pt and/or Pd) to compare the mass activity (MA) of the various catalysts, as shown in Fig. S4.† Of the five samples, the $Pd_2@Pt_1$/CNT exhibits the highest MA, followed by $Pd_4@Pt_1$/CNT and then $Pd_8@Pt_1$/CNT; the Pd/CNT catalyst was the lowest. If only the Pt mass is taken into account, the MA of the $Pd_2@Pt_1$/CNT (1.98 A mg_{Pt}^{-1}) is 9 times higher than that of the state-of-the-art Pt/C catalyst.

Although the Pd/CNT exhibits the lowest activity for the ORR, as indicated by the highest H_2O_2 yield and the most negative half-wave potential, the Pd@Pt/CNTs, especially $Pd_2@Pt_1$/CNT, exhibit enhanced catalysis for the ORR, exceeding that of the state-of-the-art Pt/C catalysts. As previously mentioned, the Pd core may be not completely overlapped by the Pt shell in the Pd@Pt/CNT. Some of the Pd core could be exposed to the exterior, in which case, a synergistic catalysis of the Pt and Pd for the ORR may occur for the Pd@Pt/CNT. To clarify the mechanism behind this phenomenon, density functional theory (DFT) calculations were performed using the DMol3

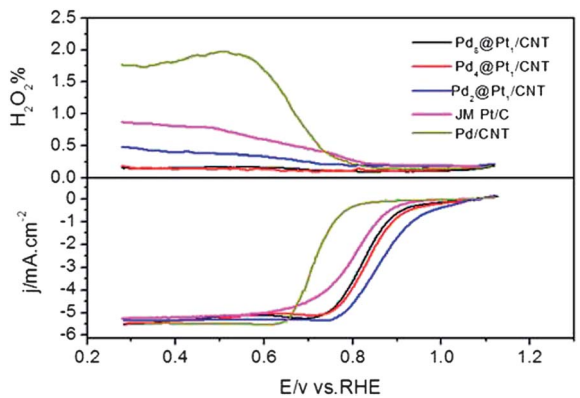

Fig. 3 ORR polarization plots (bottom) and the H_2O_2 yield plots (top) measured on the $Pd_n@Pt_m$/CNT, Pd/CNT and Pt/C-coated RRDE in O_2-saturated 0.1 M $HClO_4$ at 25 °C with an RRDE rotation rate of 1600 rpm, a voltage sweep rate of 10 mV s^{-1}, and a ring potential fixed at 0.8 V for collecting H_2O_2 with further current reductions. The ring and disk areas are 0.126 and 0.19625 cm^2, respectively. The collection efficiency of the RRDE is 37%. The Pt and Pd loadings on the RRDE for the $Pd_n@Pt_m$/CNT, JM-Pt/C and Pd/CNT are 10.2 μg cm^{-2}.

Table 1 The half-wave potential of the ORR and H_2O_2 yield on the RRDE catalyzed by Pt/C, Pd/CNT and Pd@Pt/CNT

Catalyst	Half-wave potential (V)	H_2O_2 yield (%)
Pt/C	0.795	1.05
Pd/CNT	0.715	1.77
$Pd_2@Pt_1$/CNT	0.867	0.583
$Pd_4@Pt_1$/CNT	0.833	0.295
$Pd_8@Pt_1$/CNT	0.822	0.148

Table 2 The adsorption energy and bond length of the oxygen-containing species on pure Pt and Pd and on the near-surface PtPd alloy

	Pure metal		Near-surface alloy		
Calculated parameters	Pt	Pd	Pt_3Pd	PtPd	Pd_3Pt
AE_{HOO} (eV)	1.22	1.31	0.97	1.33	1.42
AE_{O_2} (eV)	1.21	1.78	0.61	0.77	0.70
AE_O (eV)	3.60	3.61	3.37	3.39	3.53
d_{HO-O} (Å)	1.34	1.46	1.44	1.41	1.47
d_{O-O} (Å)	1.35	1.33	1.36	1.37	1.36

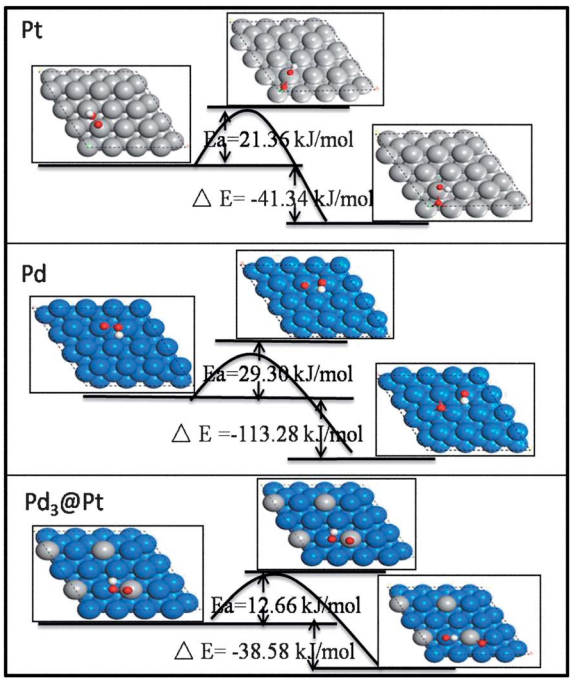

Fig. 4 The dissociation energy of the HOO* species on pure Pt and Pd and on the near-surface Pd_3Pt alloy.

software package. We used a PdPt near-surface alloy to simulate the Pd@Pt/CNTs, in which a 4 × 4 unit cell with three-layer slab models were periodically repeated within the supercell geometry containing five equivalent vacuum layers between any two successive metal slabs.[40,41] The Pd atoms in the bottom layer were fixed/frozen, and the Pd atoms in the middle layer and the Pd and Pt atoms in the top layer were relaxed, as indicated in Fig. S5.†[42] It has been proven that the effect of frozen layers on surface chemisorption energies is limited.[43] Moreover, the relative efficiency has been improved and costs have been reduced by freezing the atoms in bottom layers. For single metallic Pt and Pd catalysts, all three layers consist of Pt atoms or Pd atoms only. The DFT semi-core pseudopotential approximation was used to replace the core electrons with a single effective potential to reduce the computational cost.[44] Double numerical plus polarization (DNP) basis sets were employed for the valance orbitals.[45,46] The exchange correlation contributions were treated using the generalized gradient approximation with the PW91 formulation.[47]

Two paths exist in the ORR: an incomplete O_2 reduction by a 2 electron transfer reaction producing H_2O_2, and a complete O_2 reduction by a 4 electron transfer reaction resulting in H_2O as follows:[48–50]

$$O_2 \rightarrow O_2^* \quad (1)$$

$$O_2^* + H^+ + e^- \rightarrow HOO^* \quad (2)$$

$$HOO^* + H^+ + e^- \rightarrow H_2O_2 \quad (3)$$

$$HOO^* \rightarrow HO\cdots O^* \rightarrow HO^* + O^* \quad (4)$$

$$HOO^* + H^+ \rightarrow HOOH \rightarrow HO\cdots OH \rightarrow 2HO^* \quad (5)$$

$$O^* + H^+ \rightarrow HO^* \quad (6)$$

$$HO^* + H^+ + e^- \rightarrow H_2O \quad (7)$$

Obviously, the O–O bond dissociation determines the final product, either H_2O_2 or H_2O. A good catalyst for the ORR should have suitable binding energies for various oxygen-containing species, such as HOOH*, O_2*, HOO*, HO* and O*. Despite the lack of a consensus regarding the ORR mechanism, the route must involve both the breaking of the O–O bond (regardless of whether O_2, OOH, or HOOH is involved) and the formation of an O–H bond. An active surface should contain a proper d-band center, ε_d. A surface characterized by a higher-lying ε_d tends to bind adsorbates more strongly, thereby enhancing the kinetics of any bond-dissociation reactions. In contrast, a surface with a lower-lying ε_d tends to bind adsorbates more weakly, facilitating the desorption of adsorbates and their release from the active sites.[51] Thus, the most active surface should have an intermediate ε_d value. The currently accepted view states that the adsorption of oxygen atoms on a Pt surface is too strong and inhibits the desorption of the O* species, thus hindering the ORR as indicated in Table 2. According to the model proposed by Stamenkovic *et al.*,[52] the best catalyst should bind oxygen more weakly than pure Pt by 0.2 eV. Table 2 indicates that the O* adsorption energies on the near-surface PtPd and Pt_3Pd alloys are approximately 0.2 eV lower than that on pure Pt.

This result partly explains why the Pd@Pt/CNTs are better catalysts for the ORR than pure Pt or Pd. In addition, the O–O bond length in HOO* is more elongated on the near-surface PtPd alloys than on pure Pt. The barrier energy of O–O bond cleavage in HOO* on the near-surface PtPd alloys (12.66 kJ mol^{-1}) is much smaller that on pure Pt (21.63 kJ mol^{-1}) or Pd

(29.30 kJ mol^{-1}), as shown in Fig. 4. Thus, the O–O bond in HOO* is more easily dissociated on the near-surface PtPd alloys than on the pure Pt or Pd. The results of the calculations are in good agreement with experimental values, and effectively explain why the H_2O_2 yield in the O_2 reduction reaction on Pd@Pt/CNT is much smaller than that on pure Pt or Pd. We chose Pd_3Pt as a representative for all near-surface alloys, because on this alloy HOO* has the same adsorption pattern as those on pure Pt and Pd. Therefore, the comparison is valid.

Conclusions

In summary, we developed a facile method for synthesizing Pd@Pt/CNT bimetallic or core@shell catalysts to catalyze the O_2 reduction reaction. The results indicate that the mass-specific activity of the Pd@Pt/CNT catalysts is 7–9 times higher than that of the state-of-the-art Pt/C catalysts. In addition, the H_2O_2 yield is deceased by 85.9% on the Pd@Pt/CNT catalysts over that on the Pt/C catalysts from 1.05% (Pt/C) to 0.148% (Pd@Pt/CNT). The DFT calculations utilize the adsorption energy of all oxygen-containing species and the barrier energy of HO–O bond dissociation to explain why the Pd@Pt/CNT catalysts are able to improve the catalysis of the ORR with less H_2O_2 production while using less Pt than the Pt/C catalysts. The excellent catalysis of the Pd@Pt/CNT was ascribed to the synergistic function of Pt and Pd towards the ORR. The increased catalytic activity of the Pd@Pt/CNT is likely attributable to the weakened binding energy of the O* on pure Pt in the presence of Pd, which decreases the binding energy of the O* on Pd@Pt/CNT to within the optimum range for an ideal ORR catalyst. The synthetic protocols described in this work provide unique opportunities for material design and could be applied to new materials for ORR catalysis.

Acknowledgements

This work was financially supported by the China National 973 Program (2012CB215500 and 2012CB720300), by the NSFC of China (grant no. 20936008, 21176327 and 51272297), and by the Fundamental Research Funds for the Central Universities (CDJXS10221141).

Notes and references

1 H. A. Gasteiger, S. S. Kocha, B. Sompalli and F. T. Wagner, *Appl. Catal., B*, 2005, **56**, 9.
2 J. Zhang, K. Sasaki, E. Sutter and R. R. Adzic, *Science*, 2007, **315**, 220.
3 X. W. Yu and S. Y. Ye, *J. Power Sources*, 2007, **172**, 145–154.
4 Y. Y. Shao, G. P. Yin and Y. Z. Gao, *J. Power Sources*, 2007, **171**, 558.
5 Z. W. Chen, M. Waje, W. Z. Li and Y. S. Yan, *Angew. Chem., Int. Ed.*, 2007, **46**, 4060.
6 V. Jalan and E. J. Taylor, *J. Electrochem. Soc.*, 1983, **130**, 2299.
7 M. K. Min, J. H. Cho, K. W. Cho and H. Kim, *Electrochim. Acta*, 2000, **45**, 4211.
8 M. Watanabe, K. Tsurumi, T. Mizukami, T. Nakamura and P. Stonehart, *J. Electrochem. Soc.*, 1994, **141**, 2659.
9 C. Koenigsmann, A. C. Santulli, K. P. Gong, M. B. Vukmirovic, W. P. Zhou, E. Sutter, S. S. Wong and R. R. Adzic, *J. Am. Chem. Soc.*, 2011, **133**, 9783.
10 C. Gümeci, D. U. Cearnaigh, D. J. Casadonte and C. Korzeniewski, *J. Mater. Chem. A*, 2013, **1**, 2322.
11 V. R. Stamenkovic, B. S. Mun, M. Arenz, K. J. J. Mayrhofer, C. A. Lucas, G. Wang, P. N. Ross and N. M. Markovic, *Nat. Mater.*, 2007, **6**, 241.
12 J. F. Xu, X. Y. Liu, Y. Chen, Y. M. Zhou, T. H. Lu and Y. W. Tang, *J. Mater. Chem.*, 2012, **22**, 23659.
13 H. M. Song, D. H. Anjum, R. Sougrat, M. N. Hedhili and N. M. Khashab, *J. Mater. Chem.*, 2012, **22**, 25003.
14 N. Kristian, Y. S. Yan and X. Wang, *Electrochem. Commun.*, 2008, **110**, 353.
15 S. J. Guo, Y. X. Fang, S. J. Dong and E. K. Wang, *J. Phys. Chem. C*, 2007, **111**, 17104.
16 Y. H. Xu and X. Q. Lin, *J. Power Sources*, 2007, **170**, 13.
17 Q. Yuan, Z. Y. Zhou, J. Zhuang and X. Wang, *Chem. Commun.*, 2010, **46**, 1491.
18 B. Lim, M. J. Jiang, P. H. C. Camargo, E. C. Cho, J. Tao, X. M. Lu, Y. M. Zhu and Y. Xia, *Science*, 2009, **324**, 1302.
19 J. Zhang, M. B. V. Vukmirovic, Y. Xiu, M. Mavrikakis and R. R. Adzic, *Angew. Chem., Int. Ed.*, 2005, **44**, 2132.
20 C. Koenigsmann, A. C. Santulli, K. Gong, M. B. Vukmirovic, W.-P. Zhou, E. Sutter, S. S. Wong and R. R. Adzic, *J. Am. Chem. Soc.*, 2011, **133**, 9783.
21 J. Wang, G. Yin, Y. Shao, S. Zhang, Z. Wang and Y. Gao, *J. Power Sources*, 2007, **171**, 331.
22 S. Mukerjee and S. Srinivasan, *J. Electroanal. Chem.*, 1993, **357**, 201.
23 Q. Yuan, J. Zhuang and X. Wang, *Chem. Commun.*, 2009, 6613.
24 Z. M. Zhou, Z. G. Shao, X. P. Qin, X. G. Chen, Z. D. Wei and B. L. Yi, *Int. J. Hydrogen Energy*, 2010, **35**, 1719.
25 H. Q. Li, Q. Xin, W. Z. Li, Z. H. Zhou, L. H. Jiang, S. H. Yang and G. Q. Sun, *Chem. Commun.*, 2004, 2776.
26 R. Loukrakpam, P. Chang, J. Luo, B. Fang, D. Mott, I. T. Bae, H. R. Naslund, M. H. Engelhard and C. Zhong, *Chem. Commun.*, 2010, **46**, 7184.
27 S. Sun, G. Zhang, D. Geng, Y. Chen, R. Li, M. Cai and X. Sun, *Angew. Chem., Int. Ed.*, 2011, **50**, 422.
28 A. U. Nilekar, Y. Xu, J. Zhang, M. B. Vukmirovic, K. Sasaki, R. R. Adzic and M. Mavrikakis, *Top. Catal.*, 2007, **46**, 276.
29 Y. C. Xing, M. B. Vukmirovic, W. P. Zhou, H. Karan, J. X. Wang and R. R. Adzic, *J. Phys. Chem. Lett.*, 2010, **1**, 3238.
30 J. Zhang, Y. Mo, M. B. Vukmirovic, R. Klie, K. Sasaki and R. R. Adzic, *J. Phys. Chem. B*, 2004, **108**, 10955.
31 J. Y. Kim, Y. Jo, S. K. Kook, S. Lee and H. C. Choi, *J. Mol. Catal. A: Chem.*, 2010, **323**, 28.
32 Y. L. Hsin, K. C. Hwang and C. T. Yeh, *J. Am. Chem. Soc.*, 2007, **129**, 9999.
33 X. Li and I. M. Hsing, *Electrochim. Acta*, 2006, **51**, 5250.
34 L. Li, S. G. Chen, Z. D. Wei, X. Q. Qi, M. R. Xia and Y. Q. Wang, *Phys. Chem. Chem. Phys.*, 2012, **14**, 16581.

35 S. G. Chen, Z. D. Wei, L. Guo, W. Ding, L. C. Dong, P. K. Shen, X. Q. Qi and L. Li, *Chem. Commun.*, 2011, **47**, 10984.
36 L. C. Ciacchi, W. Pompe and A. D. Vita, *J. Phys. Chem. B*, 2003, **107**, 1755.
37 Y. J. Song, Y. Yang, C. J. Medforth, E. Pereira, A. K. Singh, H. F. Xu, Y. B. Jiang, C. J. Brinker, F. van Swol and J. A. Shelnutt, *J. Am. Chem. Soc.*, 2004, **126**, 635.
38 J. Chen, T. Herricks and Y. Xia, *Angew. Chem., Int. Ed.*, 2005, **44**, 2589.
39 X. Teng, X. Liang, S. Maksimuk and H. Yang, *Small*, 2006, **2**, 249.
40 B. Lim, X. M. Lu, M. J. Jiang, P. H. C. Camargo, E. C. Cho, E. P. Lee and Y. N. Xia, *Nano Lett.*, 2008, **8**, 4043.
41 J. Greeley and J. K. Nørskov, *J. Phys. Chem. C*, 2009, **113**, 4932.
42 T. Jacob and W. A. Goddard III, *J. Am. Chem. Soc.*, 2004, **126**, 9360.
43 N. Martsinovich, D. R. Jones and A. Trois, *J. Phys. Chem. C*, 2010, **114**, 22659.
44 B. Delley, *Phys. Rev. B: Condens. Matter Mater. Phys.*, 2002, **66**, 155125.
45 B. Delley, *J. Chem. Phys.*, 2000, **113**, 7756.
46 B. Delley, *J. Chem. Phys.*, 1990, **92**, 508.
47 J. P. Perdew and Y. Wang, *Phys. Rev. B: Condens. Matter Mater. Phys.*, 1992, **45**, 13244.
48 J. Prakash and A. T. Donald, *J. Electrochem. Soc.*, 1999, **146**, 4145.
49 D. H. Lim and J. Wilcox, *J. Phys. Chem. C*, 2012, **116**, 3653.
50 D. H. Lim and J. Wilcox, *J. Phys. Chem. C*, 2011, **115**, 22742.
51 B. Hammer and J. K. Nørskov, *Adv. Catal.*, 2000, **45**, 71.
52 V. Stamenkovic, B. S. Mun, K. J. J. Mayrhofer, P. N. Ross, N. M. Markovic, J. Rossmeisl, J. Greeley and J. K. Nørskov, *Angew. Chem., Int. Ed.*, 2006, **45**, 2897.

